Supplement of Atmos. Chem. Phys., 25, 14719–14734, 2025 https://doi.org/10.5194/acp-25-14719-2025-supplement © Author(s) 2025. CC BY 4.0 License.





Supplement of

Thermospheric nitric oxide is modulated by the ratio of atomic to molecular oxygen and thermospheric dynamics during solar minimum

Miriam Sinnhuber et al.

Correspondence to: Miriam Sinnhuber (miriam.sinnhuber@kit.edu)

The copyright of individual parts of the supplement might differ from the article licence.

S1 Supplementary material: Observations

S1.1 Nitric oxide NO

SCIAMACHY observed resonance fluorescence of NO in the γ band emissions, scanning up to 150 km every 15 days (MLT mode), overlapping with MIPAS MA/UA observations once per month (Bender et al., 2013, 2015). Data are gridded along the orbit, and daily zonal means have been calculated for daytime (sza \leq 88°) with averaging kernel diagonal element \geq 0.02. As SCIAMACHY observations depend on solar light, no night-time data or data in polar night are available. SCIAMACHY data are therefore used only for comparison against the **Long** model experiment.

S1.2 Electron density

Electron densities are provided from radio occultation observations by FORMOSAT-3/COSMIC-1, which are freely available at https://data.cosmic.ucar.edu/gnss-ro/cosmic1/repro2021/level2/. The orbit of the FORMOSAT-3 satellites has an inclination of 72°, so observations at high latitudes are sparse compared to mid- and low-latitudes. In the altitude range 90–120 km, sporadic E-layers frequently occur particularly during local afternoon in mid-latitude summer. These result in enhancements of the electron density in sharp, distinctive layers (e.g. Arras et al., 2022). In low latitudes, ionospheric scintillations are associated with a strong variation of the electron density leading to very low or even negative values in the observed density profile (e.g. Kepkar et al., 2020). The scintillations are frequently caused by equatorial plasma depletions in the F–region at altitudes between 250–500 km that predominantly occur after sunset. Both processes are not considered in the ion chemistry schemes of the models used here. To emulate the model output on noon of January 9, 2010, all observations of January 9, 2010, were therefore screened in the following way. In a first step, only observations with local solar times between 9-15 hours were selected. All individual profiles with values ≤ zero or NaNs between 92 km and 205 km were rejected, as were all profiles with vertical gradients from one vertical layer to the next of more than 35 % of a running mean over 7 vertical layers. In this way, smooth daily average profiles around local noon are provided (see upper left panel of Fig. S2). Note the limited coverage of high latitudes as well as a data gap in the Northern subtropics, which is due to the local time sampling.

S2 Supplementary material: Model-measurement intercomparisons

S2.1 Assessment of modelled NO, January-December 2010

In Figure S1, model results of NO from all five models are shown compared against NO observations from MIPAS and SCIAMACHY for the year 2010 in two latitude bins: in the tropics (0-10°N), and in high Northern latitudes (70-80°N). MIPAS data are means of am (dayside) and pm (nightside) measurements. SCIAMACHY data are am (dayside) only. Model results are averaged over the whole day. A comparison of MIPAS am and pm data shows differences generally within a factor of two, with sporadically larger differences up to a factor of 10 presumably related to differences in sampling on the dayside and nightside of the orbit (not shown); systematic order-of-magnitude differences due to the difference in daily averaging are therefore not expected.

In the low latitude lower thermosphere, NO is formed mainly by photoionization in the EUV and X-ray spectral range. Both observational data-sets show a distinct layer of NO between 10^{-2} and 10^{-5} hPa, with largest values of $(2.5-7.5)\times10^7$ cm⁻³. The temporal coverage is different between MIPAS and SCIAMACHY, and SCIAMACHY data are daytime only; also SCIAMACHY data appear to be more noisy and show more variability in particular in the vertical structure. Despite this, both observational data-sets agree both quantitatively and morphologically very well. The models also all show clear NO layers in the lower tropical thermosphere with little temporal variation. However, the size, position and strength of the NO layer is different from the observations. In WACCM-X, the absolute numbers of the NO layer are captured quite well, being in the range of $(2.5-5)\times10^7$ cm⁻³. However, the NO layer is more narrow in altitude, clearly confined to 10^{-3} - 10^{-4} hPa, so the overall amount of NO is probably lower than in the observations. Results from all other models show significantly higher NO values than the observations, with highest values of $(1-2.5)\times10^8$ cm⁻³ in HAMMONIA and WACCM-D. EMAC and KASIMA reach

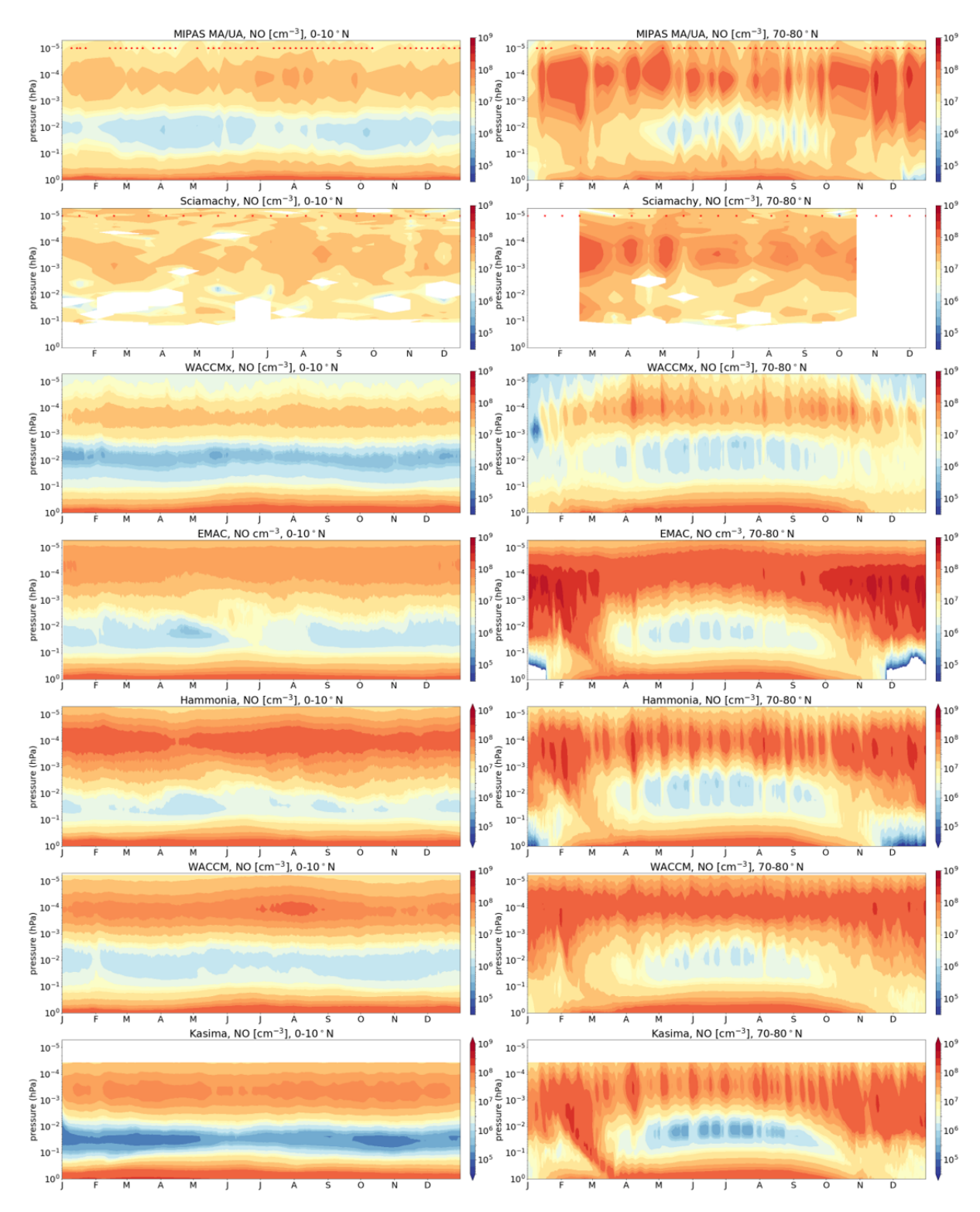


Figure S1. Zonal mean daily mean NO in the lower thermosphere throughout the year 2010. Left: tropics (0-10°N). Right: high Northern latitudes (70-80°N). From top to bottom: MIPAS observations, SCIAMACHY observations, model results from WACCM-X, EMAC, HAMMONIA, WACCM-D and KASIMA. SCIAMACHY data are 10 am lecal solar time in the illuminated part of the orbit, MIPAS is the mean of 10am/pm observations, and the model results are true daily averages.

maximal values of $(7.5-10)\times10^7$ cm⁻³. In EMAC and HAMMONIA, the NO maximum is broader than in the observations, reaching further up into the lower thermosphere.

At high latitudes, observations also show a distinctive NO layer in the lower thermosphere with higher maximal values, up to $(1-2.5)\times10^8$ cm⁻³ during spring to autumn, up to $(2.5-5)\times10^8$ cm⁻³ during November and December 2010 (only covered by MIPAS). Enhanced values of NO of up to (2.5-5)×10⁸ cm⁻³ (MIPAS) respectively up to (7.5-10)×10⁸ cm⁻³ (SCIAMACHY) are observed in the upper mesosphere in February and March 2010, indicating downward coupling via transport or mixing across the polar winter mesopause. The models qualitatively show a similar behaviour, with higher values in the lower thermospheric NO layer at high latitudes than in the tropics, and downward coupling into the upper mesosphere in February 2010 there. WACCM-X clearly underestimates NO in the high latitude lower thermosphere particularly during polar winter, with values falling below $1 \times 10^6 \text{ cm}^{-3}$ in early January, for a short period even below $1 \times 10^5 \text{ cm}^{-3}$. All other models show too high values in the thermospheric NO layer, with highest values of up to (5-7.5)×10⁸ cm⁻³ reached in EMAC. WACCM-D shows good agreement during polar winter, but too high values compared to observations during the summer season; KASIMA shows good agreement during summer, but too high values during winter. HAMMONIA generally agrees well apart from short episodes of higher NO during one to two days which might be due in part to the low temporal sampling of the observations. EMAC and WACCM-D show relatively constant values over the summer period, while HAMMONIA, KASIMA and WACCM-X show a higher amount of day-to-day variability which is more consistent with the observed variability. The mesospheric intrusion of NO during March 2010 is overestimated by most models, with highest values shown by EMAC, good agreement with MIPAS observations shown by WACCM-D and HAMMONIA, and too low values shown by WACCM-X.

In summary, all models reproduce the main features of the thermospheric NO variability, showing a distinct thermospheric NO layer roughly in the correct pressure region, with higher values at high latitudes than at low latitudes, and with an intrusion from the thermospheric NO layer into the upper mesosphere during polar spring. However, all models fail to reproduce the observations in the upper mesosphere and lower thermosphere quantitatively. The best quantitative agreement in low latitudes and during polar summer is provided by WACCM-X, which however underestimates NO during high-latitude winter by orders of magnitude. All other models show too high values of NO in the lower thermospheric NO layer, leading to an overestimation of the mesospheric intrusion during late winter. The qualitative and quantitative difference between WACCM-X and all other models is particularly noteworthy as WACCM-X uses the same parameterizations for auroral and EUV photoionization and the same photochemistry scheme as WACCM-D. This suggests that the source of the large discrepancies in lower thermospheric NO between WACCM-X and WACCM-D (and by inference, also to the other models) lies in the mid-thermosphere, above the top altitude of WACCM-D.

S2.2 Electron densities as a measure of ionization rate

60

In the upper left panel of Figure S2, electron densities in the lower thermosphere from COSMIC-1 are shown as a latitude/altitude cross-section for January 9, 2010. Due to the orbit of the FORMOSAT-3 satellites with an inclination of 72°, coverage of the auroral regions is limited to the outer edge of the Southern auroral oval. Observational gaps in Northern low latitudes are due to the local time sampling. Not considering sporadic E-layers and ionospheric scintillations, the observed distribution of electron density in the lower and mid-thermosphere between 90-200 km is fairly regular, with a steep increase in altitude below, but a slow increase in altitude above 100 km, a decrease of values into polar night in high Northern latitudes, and maximal values in 60-0°S in 140-180 km altitude. All models qualitatively reproduce this behaviour; a latitude/altitude cross section of the same day is shown at 12 UT along the 0° meridian exemplarily for WACCM-X. For a quantitative comparison, model results from all models but KASIMA, which does not explicitly consider ion chemistry, are shown at high and low Southern latitudes (0-10°S and 60-70°S), compared with COSMIC-1 data averaged over the same latitude regions. The vertical structure of the electron density is reproduced qualitatively well by all models. However, in 100-120 km, all models underestimate electron densities in both latitude bins by 10-50%. In 120-140/160 km altitude, WACCM-D, HAMMONIA (140 km) and EMAC (160 km) are within the error range of the observations, though lower than the mean value, while WACCM-X in this altitude range has lower values, just outside the error range of the observations. Above these altitudes, HAMMONIA and EMAC show significantly lower values than the observations, while WACCM-X is in very good agreement.

Electron densities and ionization rates in the lower thermosphere are closely correlated (compare lower middle and right panels to upper middle and right panels of Figure S2), forming a compact log-log distribution (not shown). This suggests that

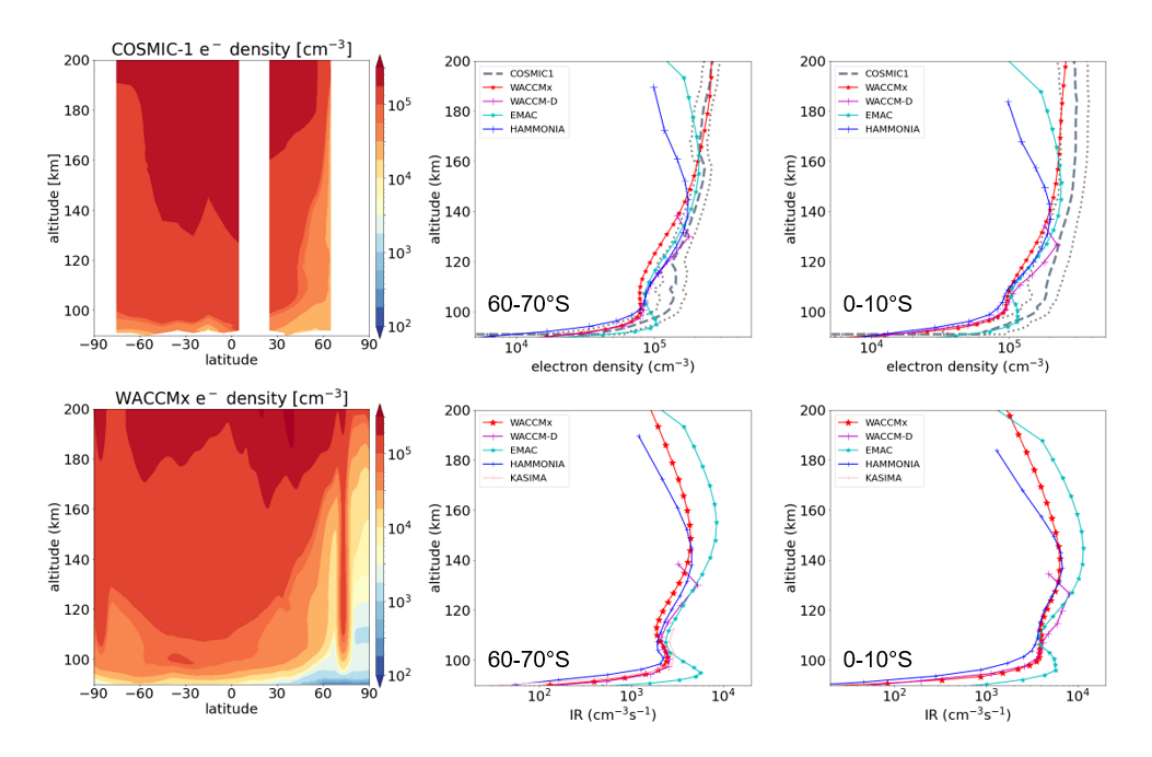


Figure S2. Upper panels, left: daily mean (9-15 LST) zonal mean electron densities from COSMIC-1 on Januar 9, 2010, after correction for sporadic-E and scintillations. Upper middle and right panels: comparison of COSMIC-1 electron densities zonally averaged for local times 9-15 hours at $60-70^{\circ}$ S (middle) and $0-10^{\circ}$ S (right) with model results of the **Snapshot** model experiment at 12:00 UTC, 0° E, averaged over the same 10° wide latitude bins. The light gray lines denote the COSMIC-1 3 σ standard error of the mean. Lower panels, left: WACCM-X electron density at 12:00 UTC, 0° E on January 9, 2010. Lower panels, middle and right: total (particle and photo-) ionization rates of the models at 12:00 UTC, 0° E, for $0-10^{\circ}$ N and $60-70^{\circ}$ S.

electron densities can be used as an indicator of the rate of ionization in the lower thermosphere. In this sense, in 100-120 km altitude, all models likely underestimate the rate of ionization, but are roughly in agreement above, with a better agreement of WACCM-D, HAMMONIA and EMAC in 120-140/160 km, a better agreement of WACCM-X above these altitudes. In the latitude ranges shown here, ionization is mainly due to EUV photoionization, and the underestimation of the electron densities in 100-120 km altitude, as well as the distinct peaks in atmospheric ionization below this altitude in 90-100 km in all models, might indicate a systematic problem either of the EUV photoionization parameterization, or of the radiative transfer, in all models. However, as all models are in agreement to, or lower than, the electron density observations, the ionization rates are likely not the reason for the overestimation of nitric oxide in the lower thermosphere by WACCM-D, HAMMONIA and EMAC shown in the previous Section S2.1.

S3 Supplementary material: Photochemical formation and loss of N(⁴S), N(²D) and NO including HAMMONIA, WACCM-D and KASIMA

100 The **Snapshot** model results of NO, N(⁴S), N(²D) and NO lifetime along 0°E on 12:00 UTC on January 9, 2010, are provided for all models in Fig. S3.

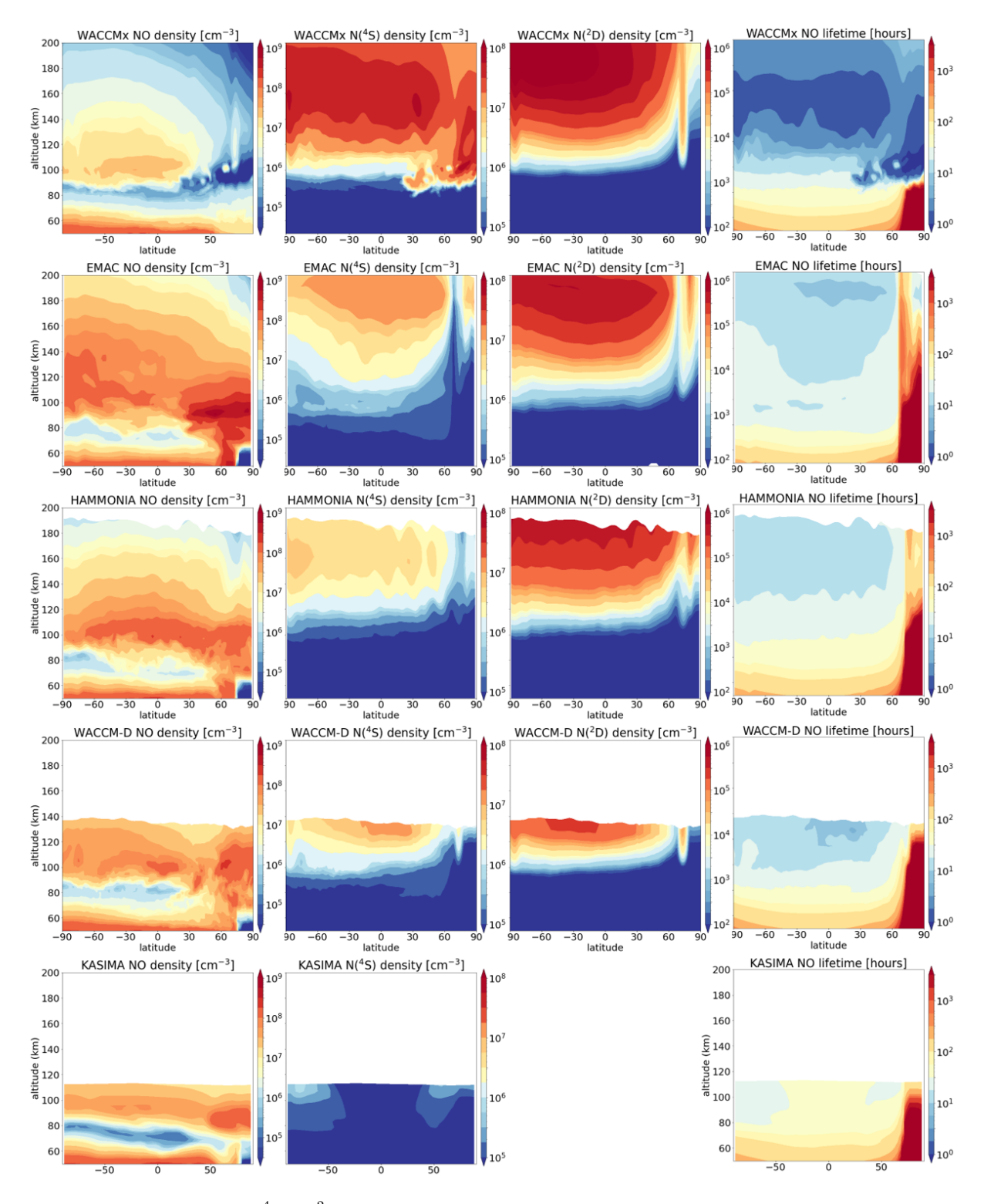


Figure S3. Snapshots of NO (left), $N(^4S)$, $N(^2D)$, and the photochemical lifetime of NO from the **Snapshot** model experiment on January 9, 2010, 12:00 UTC, at $0^{\circ}E$. From top to bottom: WACCM-X, HAMMONIA, WACCM-D and KASIMA. Note KASIMA does not consider $N(^2D)$ explicitly, but instead assumes that all $N(^2D)$ immediately form NO.

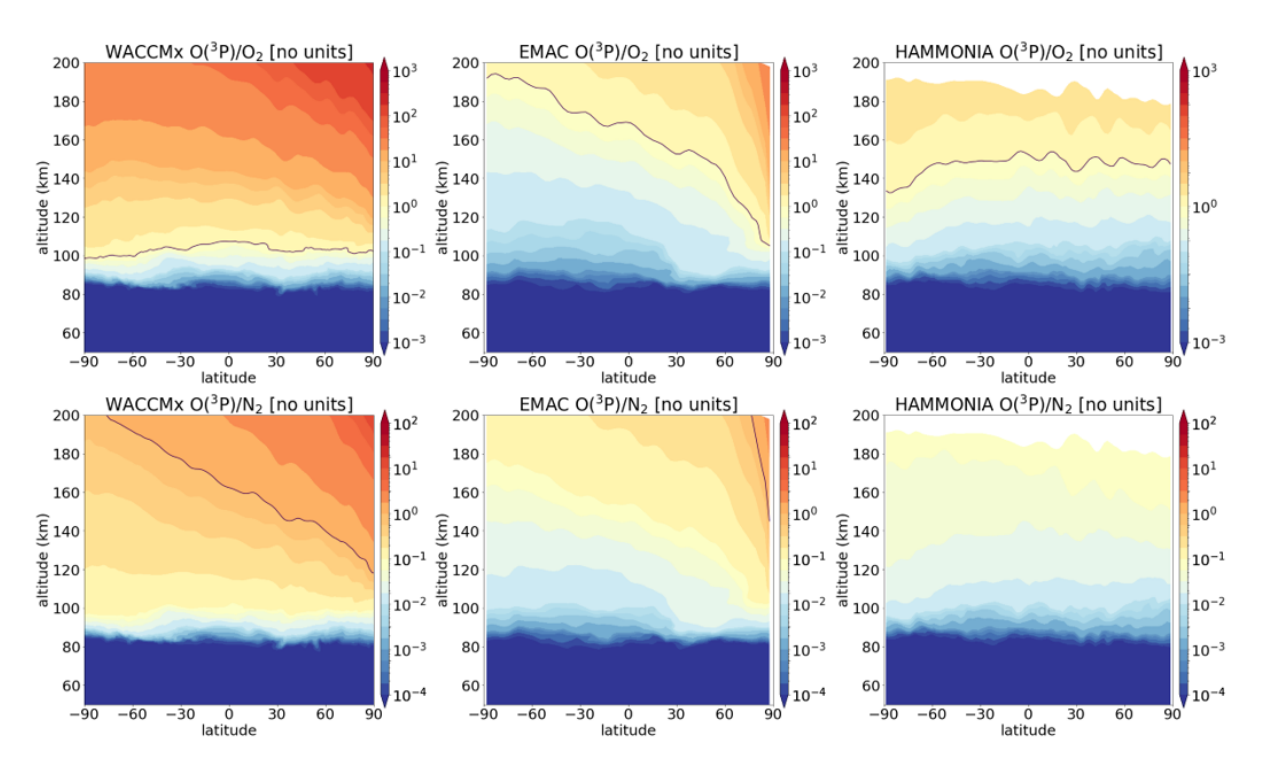


Figure S4. Ratio of O to O_2 (top) and O to N_2 (bottom) for (from left to right) WACCM-X, EMAC, and HAMMONIA. **Snapshot** model experiment on January 9, 2010, 12:00 UTC and 0° E.

S4 Supplementary material: The ratio of O to N₂ as an indicator of motion in the thermosphere

The ratio of O to N₂ is commonly used as an indicator of vertical motions in the lower thermosphere (e.g., Fuller-Rowell, 1998). One advantage of using the O to N₂ ratio is that observations of the thermospheric column of this ratio are available for model evaluation, e.g., from GUVI/TIMED (https://guvitimed.jhuapl.edu/). However, those observations do not cover high Northern latitudes on January 9, 2010, so can not be used here. Another aspect to note is that the O to N₂ ratio is affected not only by the rate of photodissociation of O₂ forming O, but also by the treatment of N₂, which is very different in the three models: WACCM-X and HAMMONIA treat N₂ as a fill gas, EMAC treats N₂ as a full chemical tracer. Molecular diffusion leads to a distinct N₂ layer in the lower thermosphere in EMAC, presumably contributing to the lower O to N₂ ratio compared to WACCM-X. The O to N₂ ratio is shown for WACCM-X, EMAC, and HAMMONIA in the lower panels of Figure S4 compared to the O to O₂ ratio. Both show a mainly consistent behavior.

References

120

- Arras, C., Resende, L. C. A., Kepkar, A., Senevirathna, G., and Wickert, J.: Sporadic E layer characteristics at equatorial latitudes as observed by GNSS radio occultation measurements, Earth, Planets and Space, 163, https://doi.org/10.1186/s40623-022-01718-y, 2022.
- Bender, S., Sinnhuber, M., Burrows, J. P., Langowski, M., Funke, B., and López-Puertas, M.: Retrieval of nitric oxide in the mesosphere and lower thermosphere from SCIAMACHY limb spectra, Atmos. Meas. Tech., 6, 2521–2531, https://doi.org/10.5194/amt-6-2521-2013, 2013
 - Bender, S., Sinnhuber, M., von Clarmann, T., Stiller, G., Funke, B., López-Puertas, M., Urban, J., Pérot, K., Walker, K. A., and Burrows, J. P.: Comparison of nitric oxide measurements in the mesosphere and lower thermosphere from ACE-FTS, MIPAS, SCIAMACHY, and SMR, Atmos. Meas. Tech., 8, 4171–4195, https://doi.org/10.5194/amt-8-4171-2015, 2015.
 - Fuller-Rowell, T.: The "thermospheric spoon": A mechanism for the semi-annual density variation, JGR, 103, 3951–3956, 1998.
 - Kepkar, A., Arras, C., Wickert, J., Schuh, H., Alizadeh, M., and Tsai, L.-C.: Occurrence climatology of equatorial plasma bubbles derived using FormoSat-3 / COSMIC GPS radio occultation data, Annales Geophysicae, 38, 611–623, https://doi.org/10.5194/angeo-38-611-2020, 2020.